NIH Public Access
Author Manuscript
J Phys Chem C Nanomater Interfaces. Author manuscript; available in PMC 2013 October 25.

Published in final edited form as:
J Phys Chem C Nanomater Interfaces. 2012 October 25; 116(42): 22245–22252. doi:10.1021/jp308176f.

Evaluation of the Thermodynamic Properties of H_2 Binding in Solid State Dihydrogen Complexes $[M(\eta^2\text{-}H_2)(CO)dppe_2][BArF^{24}]$ (M = Mn, Tc, Re): an Experimental and First Principles Study

David G. Abrecht* and **Brent Fultz**
W. M. Keck Laboratory, California Institute of Technology, 1200 E California Blvd., MC 138-78, Pasadena, CA, 91125 USA

Abstract

The solid state complex $[Mn(CO)dppe_2][BArF^{24}]$ was synthesized and the thermodynamic behavior and properties of the hydrogen absorption reaction to form the dihydrogen complex $[Mn(\eta^2\text{-}H_2)dppe_2][BArF^{24}]$ were measured over the temperature range 313K-373K and pressure range 0–600 torr using the Sieverts method. The absorption behavior was accurately described by Langmuir isotherms, and enthalpy and entropy values of ΔH=−52.2 kJ/mol and ΔS=−99.6 J/mol-K for the absorption reaction were obtained from the Langmuir equilibrium constant. The observed binding strength was similar to metal hydrides and other organometallic complexes, despite rapid kinetics suggesting a site-binding mechanism similar to physisorption materials. Electronic structure calculations using the LANL2DZ-ECP basis set were performed for hydrogen absorption over the organometallic fragments $[M(CO)dppe_2]^+$ (M= Mn, Tc, Re). Langmuir isotherms derived from calculation for absorption onto the manganese fragment successfully simulated both the pressure-composition behavior and thermodynamic properties obtained from experiment. Results from calculations for the substitution of the metal center reproduced qualitative binding strength trends of 5d > 3d > 4d previously reported for the group 6 metals.

Introduction

The Kubas binding interaction, in which a hydrogen molecule binds chemically without dissociation to a coordinatively-unsaturated metal center, has received the focus of numerous research groups for its potential to improve the energetics of physisorptive hydrogen storage materials. This interaction, characterized by σ donation of electron density from the H-H bond to the metal center and π donation from the d-orbitals of the transition metal back to the σ* orbital of the hydrogen molecule, produces a stable metal-dihydrogen bond with a higher binding enthalpy than typical physisorption materials, leading to improvements in room temperature storage capacity. Early work on the use of unsaturated metal centers in metal-organic frameworks[1, 2, 3] (MOFs) and Prussian blue analogs[4] showed enhancement in the isosteric heat of adsorption by approximately 2 kJ/mol H_2 over similar materials if unsaturated metal centers were included in the framework. Later investigations aimed at exploiting Kubas binding by incorporating unsaturated metal centers into several classes of materials to improve physisorption energetics. Computational studies have dominated the efforts, with some examples being the examination of H_2 interactions in transition metal-modified fullerenes,[5, 6] decorated polymers,[7] and more traditional organometallics.[8] These studies have obtained binding energies between −20 and −60 kJ/mol. Recently, experimental attempts to design hydrogels containing Kubas sites[9] have shown experimental isosteric heats as low as −40 kJ/mol. These increases in the binding

To whom correspondence should be addressed, dabrecht@caltech.edu.

energy over more typical physisorption values of 5–10 kJ/mol represent significant improvements in materials properties for hydrogen storage applications. However, recent experimental studies[10] have also demonstrated unusual behaviors arising from the incorporation of metal centers, such as activation energies and plateaus within the isotherms, that are not typically associated with physisorption processes, prompting the need for further investigation into the mechanism of these interactions to enable rational materials design.

Evaluation of the behavior of Kubas sites in materials designed for hydrogen storage is complicated by the presence of other physisorptive binding sites that contribute to the observable sorption properties, and studies of materials exhibiting only the Kubas interaction would considerably aid analytical efforts. Such materials are represented by the class of original dihydrogen complexes first reported by Kubas et al.[11] in 1984. Unfortunately, the available thermodynamic data on direct hydrogenations to form dihydrogen complexes remains scarce. Calorimetric studies have reported solution-state binding enthalpies of ΔH° = −41.8 and −46.9 kJ/mol for the complexes $W(CO)_3(PCy_3)_2$ and $W(CO)_3(P\text{-}i\text{-}Pr_3)_2$ in toluene, respectively.[12, 13] A similiar study in THF, attempting to develop relationships between the group 6 metals in the complexes $M(CO)(PCy_3)_2$ (M=Cr, Mo, W), found ΔH° between −27.2 kJ/mol and −41.8 kJ/mol, and entropy values ΔS° between −100 and −110 J/mol-K..[14] Solid-state measurements are limited and show deviations from solution behavior, with one study giving ΔH° = −13.22 kJ/mol and ΔS° = −9.62 J/mol-K for hydrogen absorption over the complex[15] $[Ir(cod)(PPh_3)_2]SbF_6$, representing a significant reduction in binding strength and an unexpected increase in the entropy of the bound state. While most of the data are consistent with values obtained from hydrogen storage materials, the current measurements represent a wide range of metals and ligands providing different chemical properties that, apart from the systematic study performed by Gonzalez, et al. for the group 6 complexes, do not provide chemical trends to aid in the design of new materials.

Difficulties in obtaining systematic thermodynamic data for dihydrogen complexes arise from their inherent stability, with the equilibrium pressures of most known materials falling outside of acceptable ranges for traditional chemistry techniques. To help resolve these difficulties and enable the generation of systematic thermodynamic data, we used the Sieverts method to obtain experimental isotherm measurements on the interaction of hydrogen gas with the dihydrogen complex $[Mn(CO)dppe_2][BArF^{24}]$ (dppe = 1,2-bis(diphenylphosphino)ethane, $BArF^{24}$ = tetrakis-(3,5-trifluoromethyl)phenylborate). In addition, we report electronic structure calculations on the hydrogenation of the fragments $[M(CO)dppe_2]^+$ (M=Mn,Tc,Re) to examine trends in the binding energy within the group 7 metals. We interpret our results in terms of the solid-state binding mechanism for hydrogen in these materials, and show a relatively rapid and facile means to quantitatively evaluate thermodynamic properties and establish chemical trends that are useful for materials design.

Experimental

Unless otherwise stated, all reactions were performed under a dinitrogen atmosphere using either a controlled atmosphere glovebox or Schlenck line techniques. Manganese pentacarbonyl bromide, magnesium metal and sodium tetrafluoroborate were purchased from Alfa-Aesar and used without further purification. 1,2-bis(diphenylphosphino)ethane was purchased from Strem Chemicals and used without further purification. 3,5-bis(trifluoromethyl)bromobenzene was purchased from Sigma-Aldrich and was degassed using three freeze-pump-thaw cycles and dried over activated alumina before use. Research-grade gases were purchased from Matheson and used directly. All solvents were dried and deoxygenated by purging with dry dinitrogen gas for 15 minutes before passing through packed columns of activated alumina and activated copper. Mass spectroscopy of off-

gassing products was performed using a Stanford Research Systems RGA-200 residual gas analyzer with observable pressure ranges from 10^{-8} to 10^{-5} torr. After synthesis, materials were stored under dry argon in an atmosphere-controlled glovebox until used for sorption measurements.

Solution-state NMR spectra were recorded on a Varian 300MHz instrument with ^{1}H shifts reported relative to the residual solvent peak, and ^{31}P peaks reported relative to 85% H_3PO_4. Deuterated NMR solvents were purchased from Cambridge Isotopes Laboratories. Deuterated dichloromethane was vacuum distilled from a sodium/benzophenone solution before use. Deuterated acetone was vacuum distilled twice from $CaSO_4$ and stored over 4A molecular sieves before use.

Preparation of Na[BArF^{24}]

This procedure was a modification of one in the literature.[17] 3,5-bis(trifluoromethyl)bromobenzene (5 mL, 8.55 grams, 2.918 mmol) was added to a suspension of anhydrous $NaBF_4$ (0.8173 grams, 7.446 mmol) and magnesium metal (5.028 grams, 206.87 mmol, excess) in 150 mL of diethyl ether under a nitrogen atmosphere, causing the solution to turn olive-green. The suspension was stirred for 24 hours, producing an orange solution with white precipitate. The solution was exposed to air and quenched with 20 mL of saturated aqueous sodium carbonate solution, followed by filtration over a coarse frit to remove precipitated salt. The ether layer was removed, and the aqueous layer was washed with 50 mL of fresh ether. The ether layers were combined, dried over sodium sulfate and filtered. The solvent was removed *in vacuo* and the resulting residue was dissolved in benzene and distilled in a Dean-Stark apparatus under nitrogen for three hours to remove residual water. The benzene was then removed *in vacuo*, and the residue was washed with dichloromethane and filtered to produce the product as an off-white powder. ^{1}H NMR (300MHz) in d_6-acetone: δ 7.67 (s, 4H); 7.79 (t, 8H).

Preparation of *fac*-MnBr(CO)$_3$dppe

This procedure was a modification of one in the literature.[18] A solution of the phosphine ligand 1,2-bis(diphenylphosphino)ethane (dppe, 3.5326 grams, 8.866 mmol) in 100 mL benzene was added to crystalline $Mn(CO)_5Br$ (1.2180 grams, 4.430 mmol) in a 250 mL quartz roundbottom and allowed to stir for one hour, causing $Mn(CO)_5Br$ to slowly dissolve and release CO gas to produce a yellow solution containing both the remaining free ligand and the product. The compound was observed by NMR in CD_2Cl_2 but not isolated. ^{1}H NMR (300MHz) in CD_2Cl_2: δ 2.80 (m, 4H); 3.16 (m, 4H); 7.41(m, 20H). ^{31}P NMR (300MHz) in CD_2Cl_2: δ 69.6 (s).

Preparation of *trans*-MnBr(CO)dppe$_2$

This procedure was a modification of one in the literature.[18] The solution of *fac*-MnBr(CO)$_3$dppe and free ligand in benzene from the previous synthesis was irradiated with UV light for 2 hours under an evacuated headspace and strong stirring in a 250 mL fused quartz roundbottom, causing the precipitation of 0.8 grams of red-orange solid that adhered to the roundbottom walls and blocked further irradiation. The solvent was removed *in vacuo*, and the resulting residue was washed with fresh benzene and filtered to obtain the product as an orange powder. The filtrate was collected and the procedure was repeated until no additional precipitate was formed. Total yield 3.365 grams (3.506 mmol, 79.1%) on manganese. ^{1}H NMR (300MHz) in CD_2Cl_2: δ 2.52 (m, 4H); 2.80 (m, 4H); 7.04 (t, 16H); 7.10 (m, 8H); 7.22 (quart., 8H), 7.32 (m, 8H). ^{31}P NMR (300MHz) in CD_2Cl_2: δ 72.1.

Preparation of [Mn(CO)dppe$_2$][BArF^{24}]

This procedure was a modification of one in the literature. [19] Solid Na[BArF^{24}] (3.059 grams, 3.452 mmol) was mixed with solid trans-MnBr(CO)dppe$_2$ (3.266 grams, 3.403 mmol) in a 100 mL roundbottom flask and 50 mL of dichloromethane was added to the solid mixture, immediately forming an emerald green solution that was stirred for one hour. After one hour the solution was filtered over celite to remove excess insoluble Na[BArF^{24}] and bromide salts. The filtrate was collected and the solvent removed *in vacuo*, causing a color change from emerald green to aquamarine blue. The residue was redissolved in toluene, producing a green solution, and filtered to remove any remaining bromide salts. The filtrate was collected and the solvent removed *in vacuo*, producing a blue-green powder containing mixed adducts and toluene within the structure, as described by King et. al.[19] Removal of adducts and toluene was performed under high vacuum conditions at 373K until no additional toluene was observable by residual gas mass spectroscopy, producing the five-coordinate product in 90% purity. ^{1}H NMR (300MHz) in CD_2Cl_2 under argon atmosphere: δ 2.78 (s, 8H); 6.20 (s, broad, 8H); 6.95-7.40 (m, 32H); 7.56 (s, 4H); 7.73 (s, 8H). ^{31}P NMR (300MHz) in CD_2Cl_2 under argon atmosphere: δ 82.47 (s, broad).

Reaction of [Mn(CO)dppe$_2$][BArF^{24}] with H_2 for NMR spectroscopy

Confirmation of the dihydrogen absorption ability of [Mn(CO)dppe$_2$][BArF^{24}] was performed by solution NMR. CD_2Cl_2 was vacuum transferred into a J. Young tube containing solid [Mn(CO)dppe$_2$][BArF^{24}], forming a deep blue solution. One atmosphere of hydrogen gas was introduced into the tube, and upon shaking the solution rapidly turned yellow. ^{1}H NMR (300MHz) in CD_2Cl_2: δ −7.22 (s, broad, 1.5H); 2.24 (s, 4H); 2.52 (s, 4H); 6.88-7.44 (m, broad, 40H); 7.56 (s, 4H); 7.73 (s, 8H). ^{31}P NMR (300MHz) in CD_2Cl_2: δ 85.2 (s, broad).

H_2 absorption measurements

Iterative isotherm and kinetic rate measurements were performed on 2.9 grams of degassed [Mn(CO)dppe$_2$] [BArF^{24}] using a custom-built Sieverts apparatus, described in detail previously.[20] Samples were loaded into a 14 mL stainless steel reactor under an argon atmosphere and sealed before transfer to the instrument. Swagelok VCR copper filter gaskets with 2 μm stainless steel filters were used to confine the powdered sample to the reactor during measurements. After transferring the reactor to the assembly, samples were allowed to pump down overnight to 3.1×10^{-7} torr at the pump inlet before measurements were performed. Pressure on the reactor and manifold during isotherm measurements was measured using an MKS model 120AA-25000RBJ capacitance transducer with a resolution of 0.25 torr in the range of interest. Higher pressures during kinetic measurements were recorded using an MKS model 870B33PCD2GC1 capacitance transducer with a 0–3000 psi range. The time resolution of the instrument was 1500 ms during kinetic measurements.

Manifold and reactor volumes were calibrated prior to absorption measurements through iterative expansion from a calibrated volume with argon gas. Isotherms and kinetic rate measurements were recorded by expanding an equilibrated amount of hydrogen gas from the manifold into the reactor, and the quantity of hydrogen absorbed was determined by ideal gas mole balance between the two volumes after equilibration. This procedure was repeated until no additional hydrogen uptake was observed. After completion of the measurement, the reactor and manifold were evacuated to 10^{-7} torr before heating to the next temperature.

Computations

Electronic structure calculations were performed for the singlet state of the cationic fragments [M(η^2-H_2)(CO)dppe$_2$]$^+$ and [M(CO)dppe$_2$]$^+$ (M = Mn, Tc, Re), and the hydrogen

molecule using the GAMESS-US software package.[21] Geometry optimizations for the organometallic fragments were performed using fully spin-restricted (RHF) density functional theory calculations, with the B3LYP exchange-correlation functional[22, 23] and the LANL2DZ basis set.[24, 25, 26, 27] An additional *p* polarization shell for light atoms and *d* polarization shell for heavier atoms was added to augment the basis set. Effective core potentials[25, 26, 27] representing the core 10 electrons for manganese and phosphorous atoms, the core 28 electrons for technetium and the core 60 electrons for rhenium were used. SCF convergence was set to 5.0×10^{-6} for all calculations. Geometry optimizations were performed to a tolerance of 10^{-4} au.

The initial structure for $[M(\eta^2\text{-}H_2)(CO)dppe_2]^+$ was taken from structural data reported previously for the manganese compounds by King, et al.[28] Two structures representing both an "open" geometry, in which the hydrogen molecule was removed from the H_2 adduct geometry, and the rearranged "agostic" geometry reported by King et al., in which ortho hydrogens from phenyl groups on the ligands form long-range bonds with the open coordination site, were used for $[M(CO)dppe_2]^+$. Differences between the relaxed structures obtained from calculations and the reported experimental geometries for the manganese complexes were unremarkable, beyond a contraction of all bond lengths within the structure attributable to thermal effects. The H-H bond in each dihydrogen complex was found to align parallel to the phosphorus-metal-phosphorus axis, as shown by the relaxed structure for $[Mn(CO)(\eta^2\text{-}H_2)dppe_2]^+$ appearing in Figure 1.

Ab-initio ground state electronic energies were calculated using the spin-component scaled Møller-Plesset second order perturbation[29] (SCS-MP2) scheme with the LANL2DZ-ECP basis set from the optimized geometries found from DFT calculations, which has been shown by Tomàs et al. to lead to accurate calculations for dihydrogen complexes.[30, 31] To obtain thermal corrections to the energy and normal mode frequencies, the Hessian matrix for each fragment was calculated at the B3LYP/LANL2DZ-ECP level of theory using seminumerical methods, with contributions from positive and negative displacements of 0.01 bohr. Vibrational analysis in the rigid rotor approximation was performed to obtain partition functions and normal modes of the fragments, q_{tot}, at 1 atm pressure. A scaling factor of 0.96 was used for the vibrational analysis to correct known errors in the LANL2DZ basis set, consistent with common practice.[32]

The chemical potential of hydrogen gas was calculated from the partition function for the hydrogen molecule obtained from GAMESS, through the relationship:

$$\mu_{gas}(T,P) = -kT \ln\left(q_{tot}(T,P^\circ)\right) + \ln\left(\frac{P}{P^\circ}\right) \quad (1)$$

where k is Boltzmann's constant, T is the temperature in Kelvin, P is the pressure of the system, and P° is the standard pressure of the system, taken to be 1 atm. Rotational degeneracy for the hydrogen molecule is included in the calculated partition function from the GAMESS software.

The corrected energy, E, for each fragment was obtained as the sum of the ground-state energy, ε_0, and the thermal correction to the energy obtained from vibrational analysis, $\varepsilon_{corr}(T)$, which contains contributions from translational, vibrational, and rotational motions of the molecule. The binding energy of the hydrogen molecule to the organometallic site was calculated from the corrected energies as:

$$\Delta E(T) - E_{M-H_2}(T) - E_{H_2}(T) - E_M(T) \quad (2)$$

where the subscripts M-H_2, H_2, and M represent the organometallic adduct fragment, hydrogen gas, and the bare organometallic fragment, respectively.

Results and Discussion

Experimental Results

Absorption isotherms were measured for H_2 onto [Mn(CO)dppe$_2$][BArF^{24}] at temperatures of 313K, 333K, 343K, 353K, 363K, and 373K, and are shown in Figure 2. Reversible absorption capacity for all temperatures was approximately 0.35 H_2 molecules per manganese center. No irreversible absorption was observed. This capacity value was consistent throughout measurements at all temperatures, and was stable after multiple absorption/desorption cycles performed during the course of isotherm and kinetic measurements. These properties are consistent with previous reports for solid state dihydrogen materials.[15]

Initial rate kinetics measurements were performed at 298K and 318K to determine the dependence of the absorption rate on pressure and quantity absorbed. The results for 318K appear in Figure 3. The rate of change of the pressure was determined to be linearly dependent on the pressure and the remaining capacity, such that:

$$\frac{\partial P}{\partial t} = -kP(1-\theta)$$

where θ is the fraction of the reversible absorption capacity absorbed, and k is the rate constant. Rate constants for 298K and 318K were 0.3090 s^{-1} and 0.3116 s^{-1}, respectively. The Arrhenius activation energy obtained from these values is E_a = 330 J/mol, indicating a very low activation barrier to absorption.

The isotherms presented in Figure 2 do not demonstrate a maximum like with physisorptive materials, but rather achieve a stable plateau at 0.35 H_2 molecules per manganese. This behavior is particularly evident in the isotherm at 313K. The existence of the stable plateau in the experimental isotherms is consistent with total absorption[33] and indicates that hydrogen absorbs into the bulk material instead of adsorbing onto the surface. However, the absorption rate is comparable to physisorption materials, despite no additional processing used to increase the surface area of the solid or the exposure of manganese centers to the gas. This rapid absorption is likely due to the loose packing of the bulky organic ligands in the solid, which allows the small hydrogen molecule to diffuse rapidly through the structure.[28]

The rapid kinetics and high reversibility observed in the absorption process suggest a site-binding mechanism for the binding interaction of H_2 with solid [Mn(CO)dppe$_2$][BArF^{24}] that is similar to physisorptive materials. In organometallic dihydrogen complexes, the binding orientation of the ligands is considered fixed by the atomic orbitals of the metal center, producing distinct binding sites for each ligand at the metal center. The isolation of the metal centers by the organic constituents ensures both non-interacting sites and chemical uniformity, suggesting the binding interaction at each site is isoenergetic. With this interpretation of the coordination site, we investigated the binding behavior by fitting the experimental isotherms to the Langmuir model. The Langmuir isotherm model assumes an established equilibrium between a mobile phase of guest molecules and fixed sites capable of binding a single molecule, with homogeneous, non-interacting, and isoenergetic interactions, representing an appropriate description of the organometallic coordination site if the behavior is similar to other site-binding mechanisms.

For the assumed ideal gas reaction:

$$[M(CO)dppe_2][BArF^{24}]+H_2 \rightleftharpoons [M(\eta^2-H_2)(CO)dppe_2][BArF^{24}] \quad (3)$$

in which a single hydrogen molecule binds to the open coordination site on the metal, represented by *M*, the Langmuir isotherm is given by:

$$\frac{n}{N}=\frac{\alpha P}{1+\alpha P}, \quad \alpha=\frac{K_{eq}}{RT} \quad (4)$$

where *n* is the number of bound hydrogen molecules, *N* is the total number of active binding sites, *P* is the pressure of the gas in atmospheres, *R* is the universal gas constant, *T* is the system temperature in Kelvin, and K_{eq} is the equilibrium constant for Equation 3.

Langmuir fits to the experimental data are shown as the solid lines in Figure 2. The fit for 313K was obtained by varying both the total number of active binding sites, *N*, and α as fitting parameters. A value of 0.344 H_2 per manganese center was found for *N* at 313K, and was held constant for the fits at all other temperatures. The values for K_{eq} derived from the fitted values for α and the R^2 values of the fits appear in Table 1. As can be seen from the figure and the R^2 values, the Langmuir model very accurately describes hydrogen absorption by the manganese complex, indicating that the open coordination sites within [Mn(CO)dppe$_2$][BArF^{24}] interact with hydrogen gas through a site-binding mechanism.

The standard enthalpy and entropy of the absorption interaction are readily obtained from the values of the equilibrium constant in Equation 4 through the van't Hoff equation:

$$\ln K_{eq}=-\frac{\Delta H^\circ}{RT}+\frac{\Delta S^\circ}{R} \quad (5)$$

where ΔS° and ΔH° are the entropy and enthalpy of the absorption reaction, as defined by Equation 3, at standard conditions of one atmosphere pressure and 298K. A van't Hoff plot of the equilibrium constants from the Langmuir fits appears in Figure 4. Linear regression gives values of ΔH° = −52.2 kJ/mol and ΔS° = −99.6 J/mol-K for hydrogen absorption over [Mn(CO)dppe$_2$][BArF^{24}]. This enthalpy is similar to experimental values found by Gonzalez and Hoff[14] for hydrogen binding to the group 6 complexes $M(CO)_3(PCy_3)_2$ (M = Cr, Mo, W) by solution calorimetry, and represents an interaction of comparable strength to chemisorption seen in the formation of metal hydrides. In addition, a significant increase in the absorption entropy from the standard[34] −131 J/mol-K typical for hydrogen storage materials is observed. The higher enthalpy and entropy values allow [Mn(CO)dppe$_2$][BArF^{24}] to bind hydrogen effectively near room temperature while exhibiting the rapid absorption kinetics and long cycle life characteristic of physisorption materials, a combination of properties that are highly favorable for hydrogen storage applications.

The kinetic absorption behavior is consistent with observations made by Gonzalez, et al.[12] that the kinetics of absorption and dissociation of H_2 with $W(CO)_3(PCy_3)_2$ in solution were several times faster than oxidative (dissociative) addition, which also supports the site-binding model. The solution results also imply that the site-binding mechanism is not limited to the solid state. Qualitative assessments of affinities based on competitive ligand binding would thus require control of the local hydrogen concentration, particularly in solution state measurements where the concentration of dissolved hydrogen depends on the solvent used. This additional aspect needs to be considered before using such assessments to disqualify materials as potential candidates.

Computational Results

The physics of the Langmuir model are well defined at the molecular scale and calculation of the isotherms from simulated binding energies is straightforward, allowing for direct comparison between experimental and computational results to establish the accuracy of computational methods. From statistical mechanics, the fractional coverage of absorbed molecules at the binding sites in the Langmuir model is:

$$\frac{\langle n \rangle}{N} = -\left(\frac{\partial W}{\partial \mu}\right)_{\beta} = \frac{q_s e^{\beta(\mu_{gas} - \Delta E)}}{1 + q_s e^{\beta(\mu_{gas} - \Delta E)}} \quad (6)$$

where $\beta = (kT)^{-1}$, W is the grand potential of the bound system, $\langle n \rangle$ represents the ensemble average number of absorbed molecules, and $q_s e^{\beta(\mu_{gas} - \Delta E)}$ is the partition function of the molecular species at the binding site. The pressure dependence of the fractional occupancy is expressed through the chemical potential of the gas, as shown in Equation 1. The values of $\varepsilon_{corr}(T)$ obtained from GAMESS contain the contributions to the partition function from the normal modes of hydrogen at the binding site. However, because symmetry is calculated based on the entire organometallic fragment, the output from GAMESS does not treat rotational symmetry of the hydrogen molecule appropriately, and the variable q_s in Equation 6 is used as a correction term to account for degeneracy in the rotational mode.

Carbonyl stretch frequencies obtained from the vibrational analysis were found to be 1824.32, 1820.56, and 1849.69 cm^{-1} for the open configuration of $[Mn(CO)dppe_2]^+$, the agostic configuration, and $[Mn(CO)(\eta^2\text{-}H_2)dppe_2]^+$, respectively, in good agreement with the literature values.[19, 28] The standard Gibbs free energy for the transformation from the open configuration to the agnostic configuration was also calculated from the vibrational analysis, and was found to be $\Delta G^{\circ} = -39.6$ kJ/mol, similar to values found for other agostic interactions.[12]

Six primary normal modes for dihydrogen motion at the binding site were defined as the modes having the largest magnitude eigenvectors on the dihydrogen molecule as obtained from the output of vibrational analysis on each adduct fragment. For the manganese complex, these modes correlated well with literature values obtained from inelastic neutron scattering.[28] In all three cases only the rotational mode, with frequencies of 196.79 cm^{-1}, 269.2 cm^{-1}, and 556.7 cm^{-1} for Mn, Tc, and Re, respectively, was found to be significantly populated at the temperatures of interest. The symmetry of the rotational mode was determined from analysis of the components of the eigenvector associated with the atoms of the hydrogen molecule, and the mode was defined as symmetric if the x,y, and z components were opposite in sign and had differences in their magnitude of less than 0.1 millidyne/angstrom. Within this definition, dihydrogen rotational modes in the manganese and technetium adducts were found to be symmetric, while rotation in the rhenium adduct was asymmetric with respect to the center of mass of the hydrogen molecule. To correct for the degeneracy of the symmetric modes in the manganese and technetium adducts, q_s was defined such that:

$$\frac{1}{q_s} = \frac{1}{2}\left(\frac{e^{-\frac{\Theta_v}{2T}}}{1 - e^{-\frac{\Theta_v}{T}}}\right) \quad (7)$$

where $\Theta_v = h\nu/k$ is the characteristic mode temperature obtained from the rotational mode frequency, ν. This correction removes half of the mode contribution from the total partition function, accounting for the reduction in states due to symmetric rotation. For rhenium, a value of q_s=1 was used, since no degeneracy exists in the asymmetric rotation mode.

Simulated equilibrium constants and standard binding energies for absorption onto both the open and agostic configurations appear in Table 1 and Table 2, and simulated isotherms for the manganese fragment in the open geometry appear as solid lines against the experimental data in Figure 5. Simulated isotherms for the open geometry are nearly identical to fits for the experimental data, indicating that the open geometry sites are the active sites for the absorption reaction. The simulated enthalpy and entropy values, calculated from Equations 4, 5, and 6 are $\Delta H^{\circ} = -53.5$ kJ/mol and $\Delta S^{\circ} = -103.8$ J/mol-K, demonstrating that both pressure-composition behavior and thermodynamic properties can be accurately simulated through electronic structure calculations using the B3LYP/LANL2DZ level of theory for geometry optimization and vibrational analysis, and the MP2/LANL2DZ level of theory for the electronic energy used to obtain the binding energy.

Calculations for absorption onto the agostic geometry validate the observation by King et al.[28] that direct hydrogenation of the agostic manganese complex in the solid state fails under one atmosphere of hydrogen pressure. Evaluation of Equation 6 for the agostic complex at one atmosphere hydrogen pressure and 313K gives a fractional coverage of 1.443×10^{-5}, indicating that molecules in the agostic configuration do not contribute to hydrogen binding in the experimental results. The experimental result of 0.344 for the fraction of active manganese centers evidently represents the fraction of the total manganese centers in the open configuration. This number was maintained throughout all temperatures studied, indicating that no exchange between the agostic and open configurations occurs in the solid, despite the favorable value of the free energy for the agostic complex found from calculation. Solution NMR results reported by King, et al. for the same compound[19] in CH_2Cl_2 found a similar 37% of the manganese centers were active for N_2 absorption at room temperature. It is likely that the precipitation of the N_2 adduct and subsequent release of the N_2 molecule produce the open configuration in the solid state necessary for H_2 absorption. Once precipitated, the thermal stability of the active site fraction suggests that kinetic stabilization in the solid state prevents exchange between the two configurations. This stabilization would prevent hydrogen absorption over agostic complexes in the solid state even if favorable thermodynamics were predicted, due to the inability of the ligand to leave the binding site.

With the accuracy of the calculation method established, standard energies, enthalpies, and entropies were obtained from calculation for hydrogen absorption over $[Tc(CO)dppe_2]^+$ and $[Re(CO)dppe_2]^+$. These values appear in Table 2. The resulting binding enthalpies for the open configuration are similar in strength to findings for other dihydrogen complexes. The trends in the binding enthalpies and entropies in the group 7 metals from these simulations are in good agreement with the solution calorimetry results for group 6 metals reported by Gonzalez and Hoff,[14] with the enthalpy increasing as 5d > 3d > 4d. Quantitatively, the energetic difference between 3d and 4d metals matches with the value found for the group 6 metals, despite the differences in group, molecular charge, and chemical environment. A slightly lower energetic difference of 4 kJ/mol between manganese and rhenium complexes was found relative to the reported 11 kJ/mol difference between chromium and molybdenum complexes. The good quantitative agreement implies a consistent trend in the thermodynamic values within the transition metals. Unfortunately, no direct cause for this relationship was evident from the calculations. The relationships are expected to rely upon the relative σ- and π- donation ability at the metal center, a complex property dependent upon the metal-ligand interactions and geometry.[16] Although several studies have examined the governing principles behind these properties, their exact nature remains uncertain.[35, 36, 37, 38]

The individual contribution of excited rotational modes to the site entropy can be calculated from Equation 7 through the expression:

$$S_{rot}=k\left(\ln q_s+T\frac{\partial \ln q_s}{\partial T}\right) \quad (8)$$

Values for the rotational entropy of the bound state at 298K and 373K for each of the complexes appear in Table 2. Since only the bound state is considered, the value is equivalent for both the open and agostic configurations. The softer rotational mode in the manganese adduct leads to increased entropic contributions at all temperatures, and an increased dependence on temperature relative to the other two complexes. The near equivalence of the standard entropies of technetium and manganese, despite a much lower contribution from rotation of the hydrogen molecule in technetium, is due to increased contributions from other modes within the organometallic complex. The asymmetry of the rotation in the rhenium complex leads to higher contributions to the entropy than in the technetium adduct, despite the high stiffness in the mode. The much stiffer, asymmetric rotational mode in the rhenium complex, along with the higher binding enthalpy, suggest that the H_2 molecule may have undergone oxidative addition and dissociated to form the dihydride complex. However, because both hydrogen atoms remain bound to the same metal center, the assumptions of the Langmuir isotherm are not violated. Effects from this transition are modeled in the Langmuir isotherm as a contribution to the site binding energy. This allows the absorption enthalpy to be modeled accurately by the Langmuir isotherm in cases of oxidative addition, but does not allow determination of whether the compound is a dihydrogen complex or a dihydride.

Conclusions

We report experimental and computational results on the properties of dihydrogen complexes, and interpretations with the Langmuir isotherm model. Langmuir fits for the absorption of hydrogen onto $[Mn(CO)dppe_2][BArF^{24}]$ to form the dihydrogen complex $[Mn(\eta^2\text{-}H_2)(CO)dppe_2][BArF^{24}]$ were found to accurately describe the experimental pressure-composition behavior, giving an enthalpy and entropy for the binding interaction of $\Delta H^{\circ} = -52.2$ kJ/mol and $\Delta S^{\circ} = -99.6$ J/mol-K, in general agreement with previous observations of model Kubas complexes. While the complexes within this study do not meet gravimetric or volumetric capacity expectations for vehicular hydrogen storage, they exhibit a unique binding motif capable of storing hydrogen at desirable temperatures and pressures with kinetics rivaling physisorption materials. The combination of these properties holds strong promise for the development of lower weight organometallic storage materials for applications.

Computationally derived isotherms using a mixed calculation scheme of B3LYP/ LANL2DZ-ECP for geometry optimization and vibrational analysis and MP2/LANL2DZ-ECP for total energy were also found to accurately describe the experimental behavior of the manganese complex and have provided additional insight into the configuration of the active binding site and the individual contributions from configurational and rotational entropy to the binding properties. Calculations for substitution of the metal center with other group 7 metals found similar trends in the thermodynamic properties to experimental reports for group 6 metals, with increasing binding enthalpy such that 5d > 3d > 4d, suggesting an overall trend in properties for transition metals moving down the periodic table.

Acknowledgments

The authors wish to thank David Vandervelde of Caltech for his assistance with NMR experiments, and Joseph Reiter and Jason Zan at the Jet Propulsion Laboratory in Pasadena, CA for their assistance in planning thermodynamic measurements. Sieverts instrument work was performed at the Jet Propulsion Laboratory, which is operated by the California Institute of Technology under contract with NASA. The Caltech NMR facility is

partially supported by the National Institutes of Health through grant number NIH RR027690. We are grateful to the Resnick Sustainability Institute for financial support.

References

1. Liu Y, Kabbour H, Brown CM, Neumann DA, Ahn CC. Langmuir. 2008; 24:4772–4777. [PubMed: 18366228]
2. FitzGerald SA, Hopkins J, Burkholder B, Friedman M, Rowsell JLC. Phys. Review B. 2010; 81:104305.
3. Kong L, Román-Pérez G, Soler JM, Langreth DC. Phys. Rev. Letters. 2009; 103:096103.
4. Kaye SS, Long JR. J. Am. Chem. Soc. 2005; 127:6506–6507. [PubMed: 15869251]
5. Zhao Y, Kim Y, Dillon AC, Heben MJ, Zhang SB. Phys. Rev. Letters. 2005; 94:155504.
6. Sun Q, Wang Q, Jena P, Kawazee Y. J. Am. Chem. Soc. 2005; 127:14582. [PubMed: 16231905]
7. Lee H, Choi WI, Nguyen MC, Cha MH, Moon E, Ihm J. Phys. Rev. B. 2007; 76:195110.
8. Durgen E, Ciraci S, Zhou W, Yildirim T. Phys. Rev. Letters. 2006; 97:226102.
9. Hoang TKA, Morris L, Rawson JM, Trudeau ML, Antonelli DM. Chem. Mater. 2012; 24:1629–1638.
10. Simmons JM, Yildirim T, Hamaed A, Antonelli DM, Webb MI, Walsby CJ. Chem. Eur. J. 2012; 18:4170–4173. [PubMed: 22392791]
11. Kubas GJ, Ryan RR, Swanson BI, Vergamin PJ, Wasserman HJ. J. Am. Chem. Soc. 1984; 106:451–452.
12. Gonzalez AA, Zhang K, Nolan SP, de la Vega RL, Mukerjee SL, Hoff CD, Kubas GJ. Organometallics. 1988; 7:2429–2435.
13. Kubas GJ, Burns CJ, Khalsa GRK, Van Der Sluys LS, Kiss G, Hoff CD. Organometallics. 1992; 11:3390–3404.
14. Gonzalez AA, Hoff CD. Inorg. Chem. 1989; 28:4295–4297.
15. Crabtree RH, Lavin M, Bonneviot L. J. Am. Chem. Soc. 1986; 108:4032–4037.
16. Jessop PG, Morris RH. Coord. Chem. Rev. 1992; 121:155–284.
17. Reger DL, Little CA, Lamba JJS, Brown KJ. Inorg. Synth. 2004; 34:5–8.
18. Reimann RH, Singleton E. Organometallic Chem. 1972; 38:113–119.
19. King WA, Luo X-L, Scott BL, Kubas GJ, Zilm KW. J.. Am. Chem. Soc. 1996; 118:6782–6783.
20. Purewal J, Hwang S-J, Bowman RC Jr, Ronnebro E, Fultz B, Ahn C. J. Phys. Chem. C. 2008; 112:8481–8485.
21. Schmidt MW, Baldridge KK, Boatz JA, Elbert ST, Gordon MS, Jensen JH, Koseki S, Matsunaga N, Nguyen KA, Su S, WIndus TL, Dupuis M, Montgomery JA. J. Comp. Chem. 1993; 14:1347–1363.
22. Becke AD. J. Chem. Phys. 1993; 98:5648–5652.
23. Lee C, Yang W, Parr RG. Phys. Rev. B. 1988; 37:785–789.
24. Dunning, TH., Jr; Hay, PJ. Methods of Electronic Structure Theory. Schaefer, HF., III, editor. Vol. Vol. 2. New York: Plenum Press; 1977.
25. Hay PJ, Wadt WR. J. Chem. Phys. 1985; 82:270.
26. Hay PJ, Wadt WR. J. Chem. Phys. 1985; 82:299.
27. Hay PJ, Wadt WR. J. Chem. Phys. 1985; 82:284.
28. King WA, Scott BL, Eckert J, Kubas GJ. Inorg. Chem. 1999; 38:1069–1084. [PubMed: 11670887]
29. Grimme S. J. Chem. Phys. 2003; 118:9095.
30. Tomàs J, Lledós A, Jean Y. Organometallics. 1998; 17:4932–4939.
31. Tomàs J, Lledós A, Jean Y. Organometallics. 1998; 17:190–195.
32. Russell, D., III, editor. NIST Standard Reference Database Number 101, Release 15b. 2011 Aug. NIST Computational Chemistry Comparison and Benchmark Database. http://cccbdb.nist.gov/
33. Murray LJ, Dincă M, Long JR. Chem. Soc. Rev. 2009; 38:1294–1314. [PubMed: 19384439]
34. Ozolins V, Majzoub EH, Wolverton C. J. Am. Chem. Soc. 2009; 131:230–237. [PubMed: 19072157]

35. Bautista MT, Cappellani EP, Drouin SD, Morris RH, Schweitzer CT, Sella A, Zubkowski J. J. Am. Chem. Soc. 1991; 113:4876–4887.
36. Morris RH. Inorg. Chem. 1992; 31:1471–1478.
37. Maseras F, Duran M, Lledós A, Bertrán J. J. Am. Chem. Soc. 1991; 113:2879–2884.
38. Jean Y, Eisenstein O, Volatron F, Maouche B, Sefta F. J. Am. Chem. Soc. 1986; 108:6587–6592.

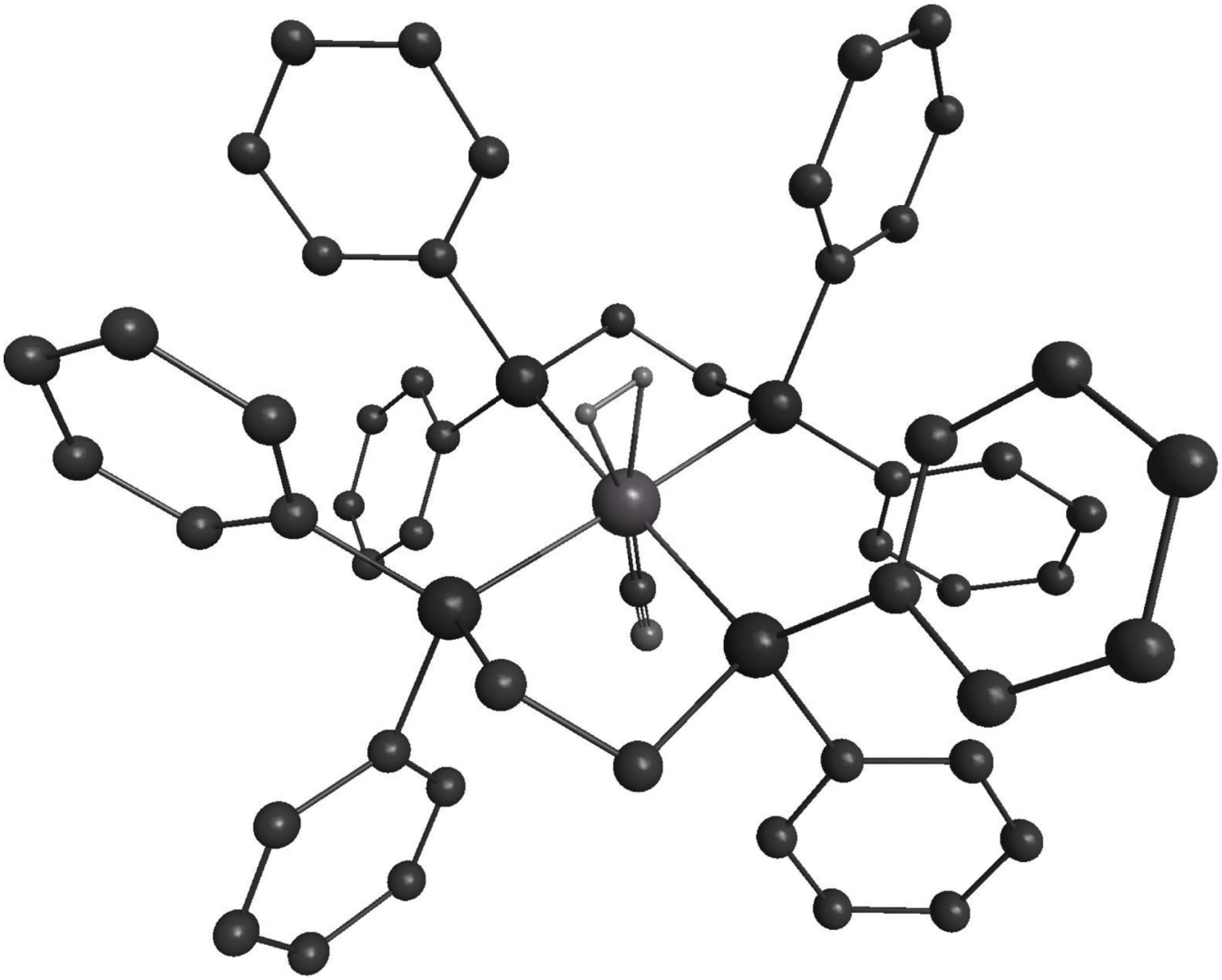

Figure 1.
Relaxed structure of the $[Mn(\eta^2\text{-}H_2)(CO)dppe_2]^+$ cation, showing the hydrogen molecule aligned along the P-Mn-P axis. Alkyl and aryl hydrogens have been removed for clarity.

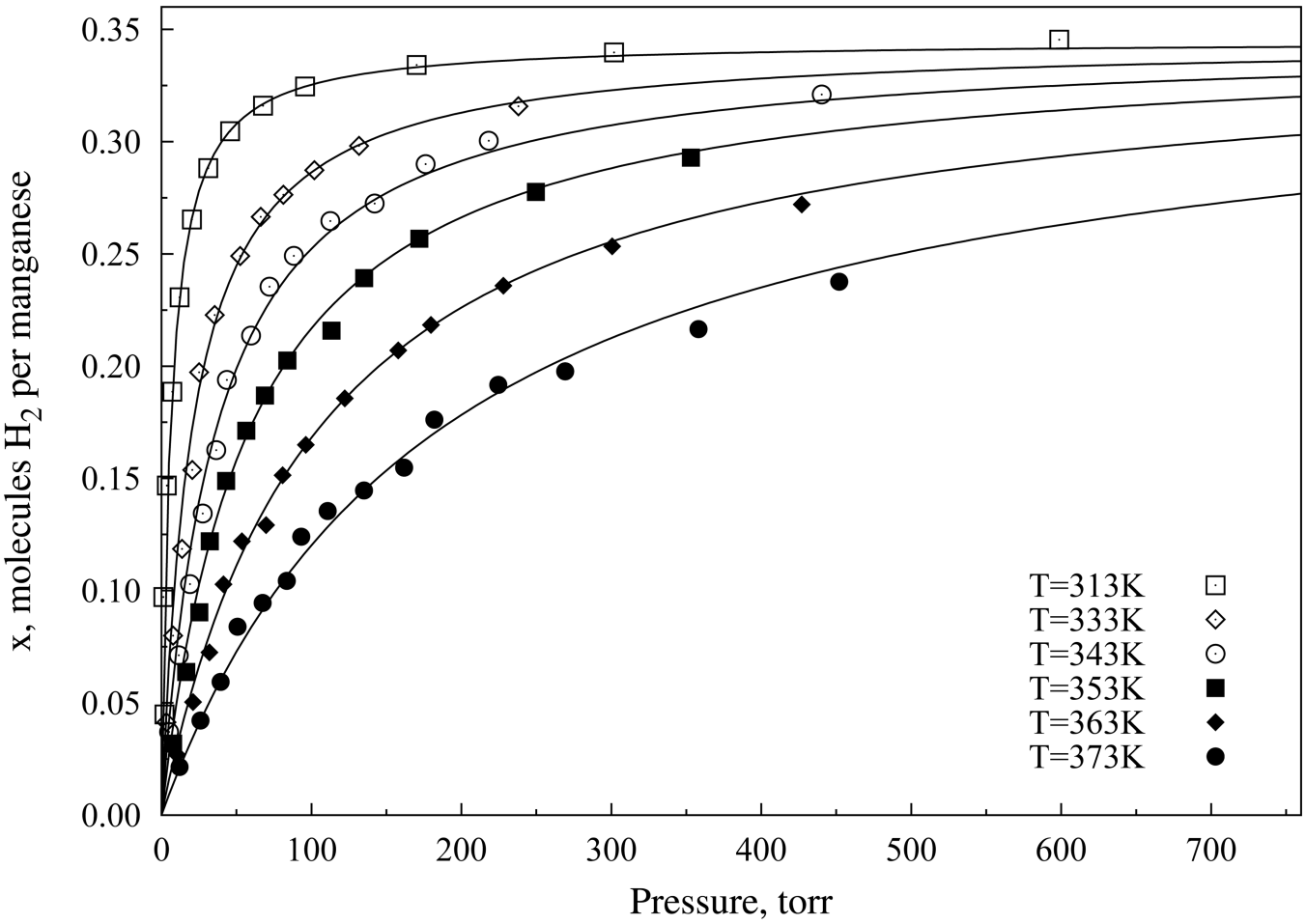

Figure 2.
Absorption isotherms for hydrogen gas onto [Mn(CO)dppe$_2$][BArF^{24}]. Solid lines are Langmuir isotherm fits to the data.

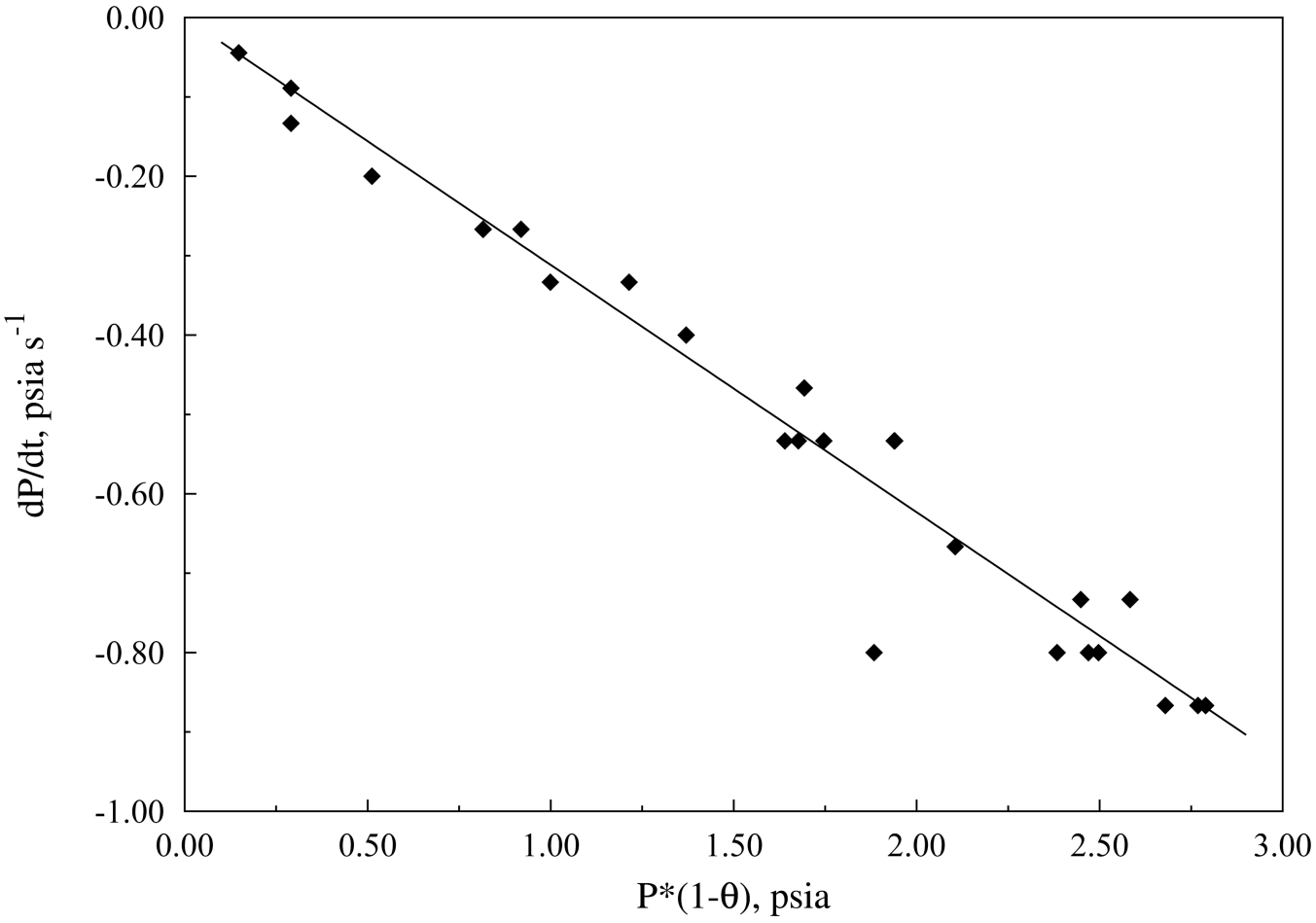

Figure 3.
Initial rate measurements for hydrogen absorption onto [Mn(CO)dppe$_2$][BArF^{24}] at 318K. Absorption kinetics were found to be linearly dependent on pressure and capacity. Linear regression gives a rate constant of k=0.3661, R^2=0.9545.

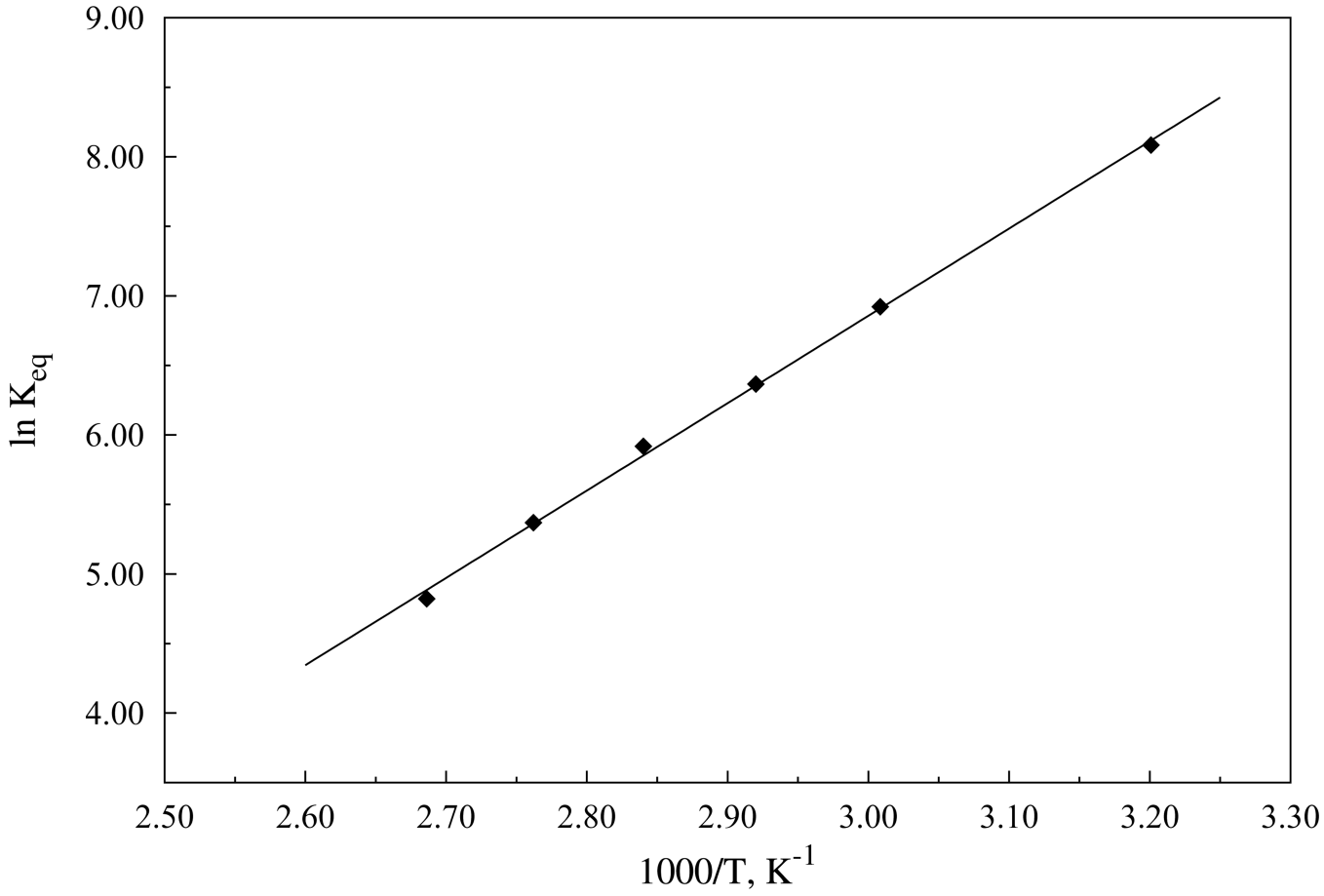

Figure 4.
Van't Hoff plot of the equilibrium constants derived from the Langmuir model. Linear regression gives ln K_{eq} = 6280.6/T - 11.986, R^2 = 0.9985, giving thermodynamic properties ΔH° = −52.2 kJ/mol and ΔS° = −99.6 J/mol-K.

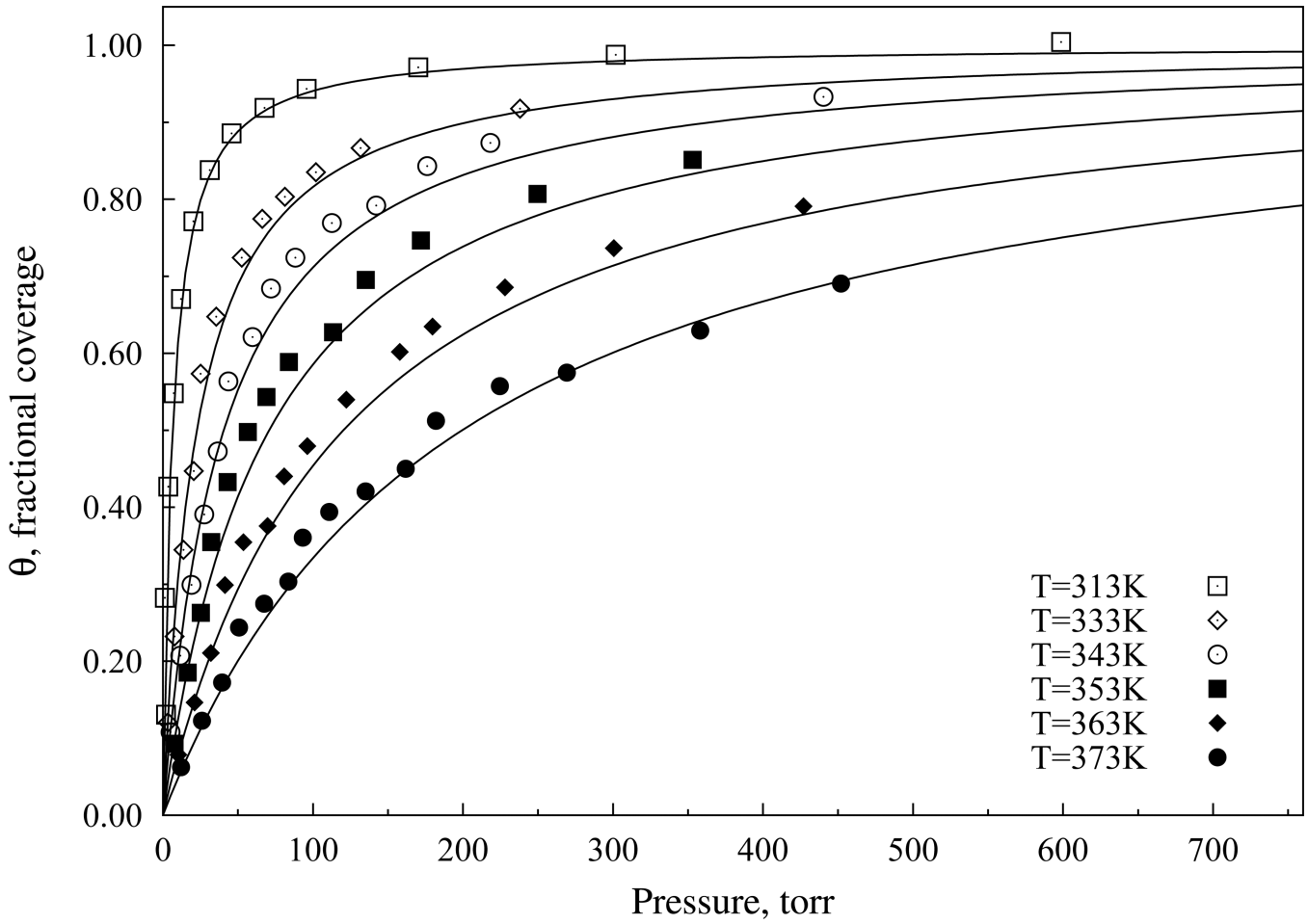

Figure 5.
Comparison of simulated isotherms for H_2 absorption onto $[Mn(CO)dppe_2]^+$ (solid black lines) to experimental data for $[Mn(CO)dppe_2][BArF^{24}]$.

Table 1

Equilibrium constants and R^2 values from experimental Langmuir fits and simulated Langmuir isotherms for H_2 absorption onto $[Mn(CO)dppe_2]^+$

Temperature	$K_{eq;exp}$, atm^{-1}	$K_{eq;sim}$, atm^{-1}	R^2_{exp}	R^2_{sim}
313K	3241.74	3117.22	0.9702	0.9692
333K	1013.12	926.34	0.9882	0.9902
343K	581.82	528.31	0.9919	0.9892
353K	371.65	309.63	0.9937	0.9766
363K	214.78	186.08	0.9962	0.9800
373K	124.19	114.37	0.9914	0.9808

Table 2

Calculated energies, enthalpies, and entropies of the H_2 absorption reaction at 1atm, 298K and rotational entropy of the bound states at 298K and 373K. Energy and enthalpy values are given in kJ/mol, and entropy values are given in J/mol-K.

Compound		ΔE°	ΔH°	ΔS°	S_{rot}(298K)	S_{rot}(373K)
$[Mn(CO)dppe_2]^+$						
	open	−43.0	−53.5	−103.8	3.20	5.04
	agostic	−1.5	−11.5	−103.9		
$[Tc(CO)dppe_2]^+$						
	open	−38.1	−49.3	−103.5	0.86	2.60
	agostic	−8.51	−18.7	−103.0		
$[Re(CO)dppe_2]^+$						
	open	−50.6	−57.5	−97.4	2.17	3.39
	agostic	−20.4	−27.1	−96.7		